Vehicle System Dynamics: International Journal of Vehicle Mechanics and Mobility

Publication details, including instructions for authors and subscription information:
http://www.tandfonline.com/loi/nvsd20

Zero-moment point determination of worst-case manoeuvres leading to vehicle wheel lift

S. Lapapong [a] , A. A. Brown [b] , K. S. Swanson [b] & S. N. Brennan [b]

[a] National Metal and Materials Technology Center (MTEC), 114 Thailand Science Park, Paholyothin Rd., Klong 1, Klong Luang, Pathumthani, 12120, Thailand

[b] Department of Mechanical and Nuclear Engineering, The Pennsylvania State University, University Park, PA, 16802, USA

Version of record first published: 16 Jul 2012

To cite this article: S. Lapapong, A. A. Brown, K. S. Swanson & S. N. Brennan (2012): Zero-moment point determination of worst-case manoeuvres leading to vehicle wheel lift, Vehicle System Dynamics: International Journal of Vehicle Mechanics and Mobility, 50:sup1, 191-214

To link to this article: http://dx.doi.org/10.1080/00423114.2012.676652

Vehicle System Dynamics
Vol. 50, Supplement, 2012, 191–214

Taylor & Francis
Taylor & Francis Group

Zero-moment point determination of worst-case manoeuvres leading to vehicle wheel lift

S. Lapapong[a], A.A. Brown[b], K.S. Swanson[b] and S.N. Brennan[b]*

[a]*National Metal and Materials Technology Center (MTEC), 114 Thailand Science Park, Paholyothin Rd., Klong 1, Klong Luang, Pathumthani 12120, Thailand;* [b]*Department of Mechanical and Nuclear Engineering, The Pennsylvania State University, University Park, PA 16802, USA*

(*Received 12 November 2011; final version received 5 March 2012*)

This paper proposes a method to evaluate vehicle rollover propensity based on a frequency-domain representation of the zero-moment point (ZMP). Unlike other rollover metrics such as the static stability factor, which is based on the steady-state behaviour, and the load transfer ratio, which requires the calculation of tyre forces, the ZMP is based on a simplified kinematic model of the vehicle and the analysis of the contact point of the vehicle relative to the edge of the support polygon. Previous work has validated the use of the ZMP experimentally in its ability to predict wheel lift in the time domain. This work explores the use of the ZMP in the frequency domain to allow a chassis designer to understand how operating conditions and vehicle parameters affect rollover propensity. The ZMP analysis is then extended to calculate worst-case sinusoidal manoeuvres that lead to untripped wheel lift, and the analysis is tested across several vehicle configurations and compared with that of the standard Toyota J manoeuvre.

Keywords: rollover; overturning; multi-body system methods; kinematic mechanics; zero-moment point

1. Introduction

According to the National Highway Traffic Safety Administration (NHTSA) [1], there were over 5.8 million crashes reported in the USA in 2008. Over 34,000 of these crashes resulted in death. While only 2.3% of crashes involve a rollover, it is responsible for 10.8% of all highway fatalities [1]. Due to the high risk of death from a rollover event, significant attention has been paid to predicting and mitigating the rollover propensity of a vehicle.

This paper proposes a novel comparative approach to evaluate vehicle rollover propensity based on the zero-moment point (ZMP) metric that is model independent. In particular, we consider a frequency-domain representation of the ZMP that utilises a simple linear vehicle dynamic model and the frequency response to qualitatively evaluate vehicle rollover propensity and to determine worst-case manoeuvre situations. The ZMP is used along with simple vehicle roll models to identify situations that could be of concern. The ZMP metric, whose details are

*Corresponding author. Email: sbrennan@psu.edu

ISSN 0042-3114 print/ISSN 1744-5159 online

http://dx.doi.org/10.1080/00423114.2012.676652
http://www.tandfonline.com

given below, has been shown in previous work by the authors [2–5] to be useful to predict wheel-lift onset on both flat and banked surfaces, even with unknown tyre forces, based solely on inertial vehicle pose measurements. The original use of the ZMP method was in the area of bipedal robots [6] to allow one to predict robot walking stability independent of the foot/ground contact force. Similarly, this paper investigates the use of the ZMP as a roll stability metric independent of the tyre/ground contact forces, using the contact polygon of the vehicle. The method is thus quite different from the load transfer ratio (LTR) method [7], which requires tyre forces to be measured or estimated.

A particular challenge in predicting rollover is the complex interplay between vehicle dynamics, the manoeuvre, and the slippage of the tyre. In previous work within the authors' research group [8], an analysis was conducted to explore whether a vehicle will skid first, or roll first, given the increasing magnitudes of the steering inputs. This work was conducted prior to the development of the ZMP, and thus it used a very simplistic metric for wheel lift. A goal of this work is to apply the ZMP algorithm to determine the skid-before-roll condition of a vehicle. Not only is this process useful for determining the rollover propensity of a vehicle under variations in forward speed, vehicle parameters and environmental conditions, but it also provides insights into determining worst-case steering manoeuvres that lead to wheel lift.

The remainder of the paper is organised as follows: Section 2 discusses the history of rollover and wheel-lift metrics. Section 3 explains the ZMP metric in detail and why it is chosen in this study. Section 4 applies the ZMP concept to commonly used rigid-body vehicle models to derive expressions predicting the rollover propensity of a vehicle. Section 5 then examines how common variations in vehicle situations affect the ZMP. Section 6 presents the calculation procedure that uses a linear model to determine the worst-case steering inputs, based on the ZMP calculations. Section 7 presents a simple vehicle dynamic model used to generate data for the ZMP calculation and representative plots for a test vehicle. Section 8 presents the results of CarSim simulations of the situations predicted to lead to wheel lift. Section 9 uses the procedure outlined in Section 6 to demonstrate the calculation of worst-case steering inputs for several vehicle situations. Section 10 then summarises the main points of the paper.

2. History of rollover and wheel-lift metrics

The most unequivocal method to determine a vehicle's rollover propensity is to experimentally measure its roll behaviour during particular driving manoeuvres, and indeed this approach is used by NHTSA to determine a vehicle's dynamic rollover resistance to untripped rollover [9]. The practical challenges of this approach are that the field tests are expensive and difficult to conduct correctly and repeatedly. Furthermore, because one cannot ever perform enough tests to represent all driving situations, the completeness of the test suite is always a concern; a 'pass' outcome under one particular test or even set of tests does not guarantee that the same vehicle would not exhibit wheel lift or rollover under some other combination of steering inputs, operating speeds, road conditions, and vehicle operating conditions that is outside the test suite.

Another approach to predict rollover propensity is to use rollover metrics that qualitatively evaluate the risk of vehicle rollover based on relatively simple experimental measurements. Many of these metrics are based on static or steady-state models of vehicle behaviour, and examples include the static stability factor (SSF) [10] or experimental tests such as side-pull test [10], tilt-table test [10], and centrifugal test [10]. Many of these metrics – particularly the SSF – are shown to correlate very well with the rollover rates of vehicles as seen in national crash databases [9]. Unfortunately, it is possible to artificially improve the SSF

with slight suspension alterations that lead to few significant changes to the roll dynamics of the vehicle [10]. Thus, a common certification practice as outlined in Transportation Recall, Enhancement, Accountability, and Documentation Act is to combine SSF measurements with experimental dynamic measurements to achieve a heuristic classification of vehicle rollover stability.

In addition to the issues mentioned previously, rollover or wheel-lift metrics based on experimental and empirical methods can be difficult to use for the design of the vehicle or subsequent control. For these situations, a model-based rollover metric is desirable so that one can predict (and react to) the worst-case operating situations. Recognising this issue, there has been a flurry of healthy research efforts utilising dynamic models to examine dynamic rollover behaviour and produce rollover metrics. Examples include the LTR [7], the lateral acceleration threshold [11], the time-to-rollover metric [12], the threshold based on roll angle [13], a rollover index that is a combination of states of the roll angle, roll rate, lateral acceleration, and time-to-wheel-lift metric [14], a rollover threshold for the suspended vehicle model [15], the dynamic stability index [15], and a stability moment [16]. One challenge in adopting these dynamic rollover metrics for the evaluation of production vehicles is that they often require vehicle situational knowledge that may be difficult to obtain, for example, tyre–pavement interaction forces, vehicle chassis model parameters, definition of the driving manoeuvres, and/or road profile. Recognising the importance of inertial parameters in model-based prediction of rollover propensity, NHTSA has compiled a database of vehicle inertial parameters that remains one of the best databases of this information to date [17]. However, even with good estimates for vehicle inertial parameters, it can be difficult to establish whether one model or modelling approach achieves a sufficient level of fidelity such that one model-based method can be established as a reliable rollover metric for all vehicles and situations. Recognising that there will always be a need for experimentation on a vehicle, the goal of this research is to determine how this experimentation can be guided by model analysis to identify the worst-case driving situations.

3. The ZMP as a roll stability metric

To measure vehicle rollover propensity, a technique called the ZMP [6] is applied in this study. By definition, the ZMP is the point on the ground where the summation of the tipping moments acting on an object, due to gravity and inertial forces, equals zero [18]. An object will remain in dynamic equilibrium if the net force vector of the object to the ground acts within the contact polygon of the object to the ground.

The novelty of the ZMP is that it ensures that the force contact point is simply the location where the net moment on the object from the ground is zero, hence the terminology 'zero-moment' point. The other key advantage of the ZMP metric is that the calculation of the ZMP does not require any information about the ground-to-object reaction forces. Using the Lagrange–d'Almert principle, if one can measure or estimate the kinematic motion of all objects in a kinematic chain of bodies, then one can calculate where the net moment contribution of each body to the ZMP is. This avoids the difficult estimation of contact forces either between the chain of objects or from the ground link to the ground surface. The location of the ZMP must be within the supporting polygon to maintain the dynamic stability of a kinematic chain; otherwise, the chain will turn over [19].

Historically, the concept of ZMP was first formally developed and introduced by Vukobratović in 1968 [6,19–21]. This concept has been very useful and is now widely used in bipedal robotics research. Biped robotics scientists have applied the concept to preserve robots' dynamic balance during walking or, in other words, to maintain robots' stability, preventing

the robots from overturning. Today, there are hundreds of biped walking robots that have been implemented with this algorithm, for instance, Honda's humanoid robots [22]. Moreover, many researchers have used the ZMP as a stability constraint for mobile manipulators to prevent the overturn of the mobile manipulators due to their own dynamics [23,24].

The utility of examining the ZMP in this study is that the proximity of the ZMP to the edge of the support polygon of a vehicle is a dynamic metric for the rollover propensity of a vehicle. Put simply, if the lateral position of the ZMP is outside the vehicle's track width, the vehicle is unstable and will experience wheel lift. The vehicle's proximity to the wheel lift can be inferred by the ZMP's distance relative to the vehicle's centreline, hereafter called y_{ZMP}, derived below. Previous work by the authors has shown that many analytical and empirical rollover metrics found in the literature are simplified forms of the y_{ZMP} calculation [4].

Additionally, the y_{ZMP} calculation is largely independent of the kinematic data source. Other than the requirement that the number of bodies modelled in the ZMP calculation be the same as the number in a kinematic chain representing the vehicle, the vehicle motion used to calculate the y_{ZMP} can occur from either experimental measurements or any choice of vehicle dynamic model. In this work, sinusoidal excitations are considered to produce calculations of the lateral location of the ZMP in the frequency domain, a process summarised in Figure 1.

To generalise the idea of the ZMP to a multi-body system, a kinematic chain shown in Figure 2 is considered. In the figure, the ith body of the kinematic chain has a mass m_i and an inertia tensor $\mathbf{I}_i$ about its centre of mass. We assume that the ith body moves with linear velocity $\vec{v}_i$ and linear acceleration $\vec{a}_i$ and rotates at angular velocity $\vec{\omega}_i$ and angular acceleration $\vec{\alpha}_i$. The centre of mass of the ith body relative to an inertial frame ($OXYZ$) is located by $\vec{r}_i$. Using

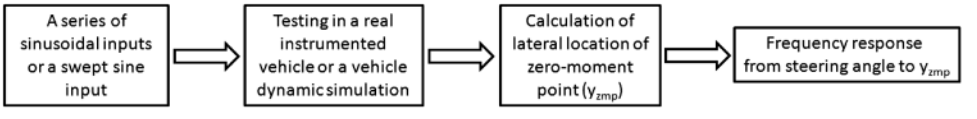

Figure 1. Process of rollover propensity evaluation.

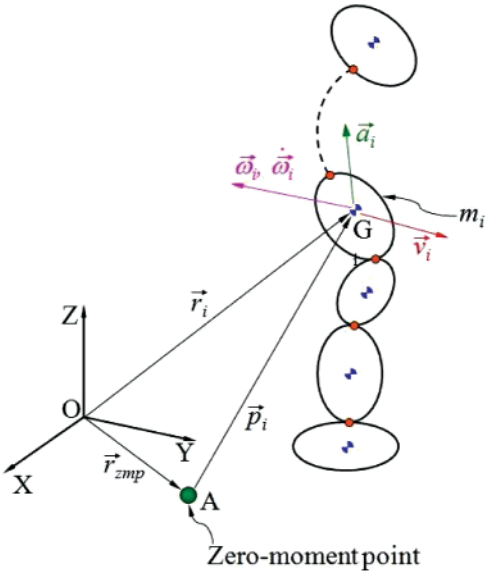

Figure 2. Kinematic chain.

general equations of motion [25–27] and d'Alembert's principle [28], the moment equation about point A in Figure 2 induced by inertial forces and gravity is

$$\vec{M}_A = \sum_i (\vec{p}_i \times m_i \vec{a}_i) + \sum_i (\mathbf{I}_i \vec{\alpha}_i + \vec{\omega}_i \times \mathbf{I}_i \vec{\omega}_i) - \sum_i (\vec{p}_i \times m_i \vec{g}), \tag{1}$$

where $\vec{p}_i = \vec{r}_i - \vec{r}_{\mathrm{ZMP}}$, $\vec{r}_{\mathrm{ZMP}}$ is the position vector of the ZMP, and $\vec{g}$ is gravitational acceleration. We note that regardless of mass-to-mass constraint forces, the gravity and inertial forces of each mass in a body must be stabilised by a net moment on the ground surface. Thus, if $\vec{M}_A = [0\ 0\ M_{A_z}]^{\mathrm{T}}$, then point A becomes a ZMP.

4. The ZMP as a vehicle rollover threat index

To apply the concept of ZMP to a vehicle system, two different kinematic chains were considered in prior work [4]: one representing a rigid vehicle and the other representing a sprung/unsprung model of a vehicle. The y_{ZMP} calculation for both the chains was found to be nearly identical in the experimental field tests; so for brevity, only the simpler rigid model is presented here. To begin, the vehicle is modelled as a rigid body as shown in Figure 3. The vehicle model shown in the figure is assumed to have no suspension and no compliance in its tyres.

In Figure 3, the coordinates $oxyz$ are fixed with the vehicle at the centre of gravity of the vehicle (point G). Point Q is a ZMP and is constrained to always be physically on the ground. To calculate the location of the ZMP, we assume that the vehicle is symmetric in the xz-plane ($I_{xy} = 0$) and the vehicle is free to move in any direction. The nomenclature used in this section is defined in Table 1 and Figures 3 and 4.

Considering a general case that the vehicle is on a banked surface as shown in Figure 4, the location of the y_{ZMP} may be expressed as

$$\vec{r}_{\mathrm{ZMP}} = x_{\mathrm{ZMP}}\vec{i} + y_{\mathrm{ZMP}}\vec{j} + \left[h + \frac{T}{2}|\tan(\phi_{\mathrm{r}} - \phi_{\mathrm{t}})| - y_{\mathrm{ZMP}}\tan(\phi_{\mathrm{r}} - \phi_{\mathrm{t}})\right]\vec{k}. \tag{2}$$

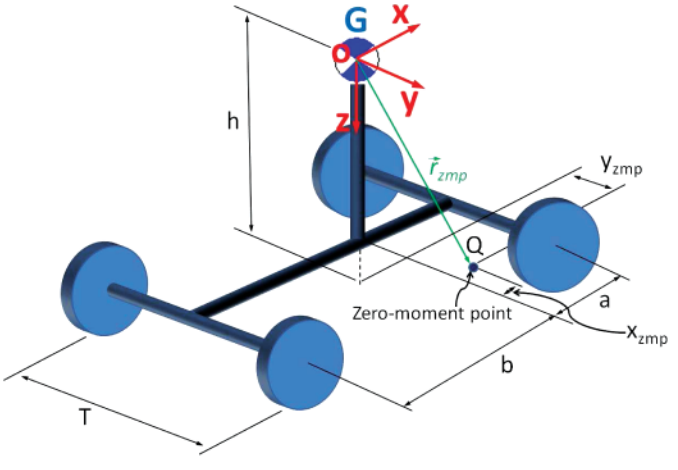

Figure 3. Rigid vehicle model.

Table 1. Nomenclature for rigid vehicle model.

Symbol	Definition	Symbol	Definition
m	Total mass of the vehicle	ω_s	Angular velocity of sprung mass
m_s	Sprung mass of the vehicle	ω_u	Angular velocity of unsprung mass
a	Distance from CG to the front axle	ϕ_r	Roll angle
b	Distance from CG to the rear axle	ϕ_t	Roll angle of terrain
h	Height of CG	θ	Pitch angle
h_s	Height of sprung mass CG	p	Roll rate
h_r	Height of roll centre	q	Pitch rate
h_{sr}	Height of sprung mass CG from roll centre	r	Yaw rate
		δ	Steering angle
T	Track width	$\lvert\delta\rvert_{max,skid}$	Max steering angle leading to tyre skidding
$I_{xx,yy,zz}$	Mass moment of inertia about the x-axis, y-axis, and z-axis	$\lvert\delta\rvert_{max,roll}$	Max steering angle leading to wheel lift
$I_{xz,yz}$	Product mass moment of inertia		
V	Lateral velocity	α	Slip angle
U	Longitudinal velocity	$\alpha_{max,skid}$	Slip angle at which skidding occurs
$C_{\alpha f}$	Front cornering stiffness		
$C_{\alpha r}$	Rear cornering stiffness	F_f	Force on the front axle
D_ϕ	Torsional damping constant	F_r	Force on the rear axle
K_ϕ	Torsional spring constant	F_z	Vertical tyre force
$\vec{i},\vec{j},\vec{k}$	Unit vector along the x-, y-, and z-axes	a_G	Acceleration at CG[a]
		r_{ZMP}	ZMP location
a_s	Acceleration of sprung mass	y_{ZMP}	ZMP location on the y-axis
a_u	Acceleration of unsprung mass		
v_s	Velocity of sprung mass	x_{ZMP}	ZMP location on the x-axis
v_u	Velocity of unsprung mass		

[a]In the derivation, the subscripts x, y, and z indicate accelerations in the x-, y-, and z-directions. CG, center of gravity.

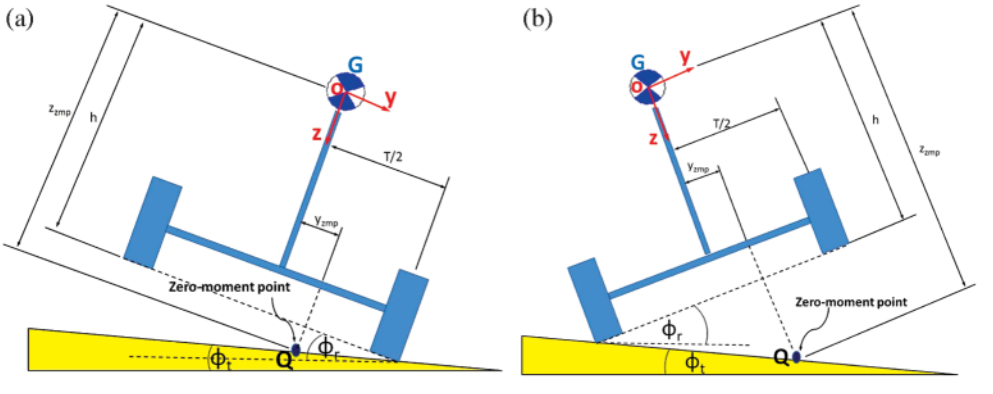

Figure 4. Rigid vehicle model on a banked surface: (a) $\phi_r \geq \phi_t$ and (b) $\phi_r < \phi_t$.

Using Equation (1), the lateral location of the ZMP can be expressed as

$$\begin{aligned} y_{ZMP} = {} & \{mg\cos(\theta)\sin(\phi_r)[T|\tan(\phi_r-\phi_t)|+2h] - ma_{Gy}[T|\tan(\phi_r-\phi_t)|+2h] \\ & - 2I_{xx}\alpha_x + 2I_{xz}\alpha_z + 2I_{yz}(q^2-r^2) \\ & + 2(I_{xz}+I_{yy}-I_{zz})qr\}/\{2m[g\cos(\theta)\cos(\phi_t)\sec(\phi_r-\phi_t) \\ & - a_{Gy}\tan(\phi_r-\phi_t) - a_{Gz}]\}. \end{aligned} \tag{3}$$

Since the main goal of this work is to determine vehicle rollover propensity, only the expression of y_{ZMP} is presented for brevity. The complete derivations of the location of the ZMP are provided in [2,4].

Additionally, the fidelity of the above equation to predict vehicle rollover was confirmed by time-domain analyses of actual wheel-lift experiments, as reported in [2–4]. During many of these sudden wheel-lift events, the test vehicle exhibited visible torsional flexibility along the two-rail truck frame. Though this flexure was not modelled, the ZMP calculation and wheel-lift prediction still showed a good agreement. Most current passenger vehicles, including modern pick-up trucks, have frames that are similar to or even stiffer than those of the test vehicle used. However, it is unclear if the ZMP would apply to an exceedingly compliant vehicle, for example, a flat-bed trailer. For cases of extreme torsion, the models mentioned above should be modified to include multi-body dynamics representative of frame-twist behaviour.

5. The effect of variations in vehicle loading, environment, and speed on the ZMP

Although the ZMP has proven to be useful for predicting wheel lift in the time domain, the utility of the ZMP extends to the frequency domain as well where one can readily obtain a comparison of vehicle designs and operating conditions and their effect on wheel lift. In this section, several different scenarios are examined to show some straightforward extensions of this approach to practical analyses. These scenarios include the following: (1) how y_{ZMP} changes with increasing speed, (2) how vehicle loading condition affects y_{ZMP}, and (3) how operation of a vehicle on a banked surface affects y_{ZMP} versus level driving. Some of these scenarios will be explored in more detail in Section 6, but the following analysis gives a qualitative picture of the effects that these parameter changes have on vehicle rollover stability.

In many of the analyses that follow, the experiments and simulations consider a vehicle burdened with extra weight. In these cases, one must recognise that the load variation on a vehicle changes more than just the mass; the inertia, centre of gravity, and tyre model parameters will also change. To obtain realistic values for different loading conditions, experimental system identification was performed on a 1989 GMC 2500 pick-up truck illustrated in Figure 5 available at the Larson Transportation Institute Test Track for both unladen and laden conditions. For the laden condition, 784 kg was added to a standard equipment rack mounted over the truck's bed, equivalent to the rated weight for the rack built for this vehicle. The parameters of the unladen truck and loaded truck are summarised in Tables 2 and 3. The mass of the unladen truck was 2279 kg and that of the laden truck was 3321 kg, which represents a mass increase of almost 50%. Due to tyre load sensitivity, the cornering stiffnesses of the same vehicle under different loads will also vary greatly as shown in Tables 2 and 3.

Experimental testing under both conditions showed that the laden truck would readily exhibit wheel lift and possibly rollover for many manoeuvres, and so outriggers were used throughout all field tests to ensure safety. Because of the danger and difficulty of physically testing the laden vehicle for wheel-lift situations, a CarSim model of the pick-up truck was also

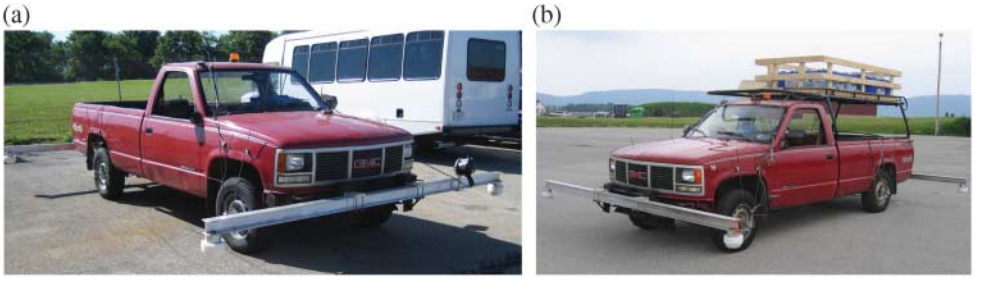

Figure 5. Test vehicles: (a) unladen test truck and (b) test truck loaded with 784 kg extra weight.

Table 2. Parameters of the unladen truck.

Symbol	Value	Unit	Symbol	Value	Unit
m	2279	kg	I_{xx}	854 kg m^2	
a	1.390	m	I_{yy}	5450	kg m^2
b	1.964	m	I_{zz}	5411	kg m^2
h	0.812	m	I_{xz}	0	kg m^2
T	1.615	m	I_{yz}	0	kg m^2
$C_{\alpha f}$	75,700	N/rad	$C_{\alpha r}$	83,600	N/rad

Table 3. Parameters of the truck with a 784 kg extra load.

Symbol	Value	Unit	Symbol	Value	Unit
m	3321	kg	I_{xx}	2030	kg m^2
a	1.894	m	I_{yy}	7751	kg m^2
b	1.460	m	I_{zz}	7862	kg m^2
h	1.220	m	I_{xz}	0	kg m^2
T	1.615	m	I_{yz}	0	kg m^2
$C_{\alpha f}$	120,000	N/rad	$C_{\alpha r}$	120,000	N/rad

created using the measured vehicle parameters; validation of this model is presented in later sections. For consistency and repeatability in the analyses that follow, a series of sinusoidal road-wheel steering inputs whose frequencies ranged from 0.1 to 3.0 Hz were simulated, and the truck's states were then used to compute the corresponding y_{ZMP}. The frequency responses from steering input to y_{ZMP} were constructed using the correlation frequency response analysis as described in [29,30].

To analyse the effect of speed variations on wheel-lift propensity, the y_{ZMP} was calculated for the unladen truck for many speeds. Figure 6 illustrates the frequency responses from steering angle to lateral location of the y_{ZMP} from the case that the longitudinal velocity of the truck is varied from 11.2 m/s (25 mph) to 26.8 m/s (60 mph). This range of speeds was chosen as it represents nearly all crash data for which vehicle rollover occurs during road departures on barrier-free highways [31]. Furthermore, the trends for higher speeds would require additional inclusion of aerodynamic effects, which is beyond the scope of this paper. The results shown in Figure 6 indicate that the truck travelling at a higher longitudinal velocity has a higher tendency to produce higher y_{ZMP} values, which can lead to a higher propensity for wheel lift. Considering the results obtained in the low-speed cases (11.2 and 13.4 m/s), the truck's rollover propensity as expressed in y_{ZMP} magnitude increases only slightly with the increasing frequency of the steering inputs. However, in the high-speed cases, both low and high frequencies will generate large y_{ZMP} magnitudes, with a notch-like characteristic observable at around 1.4 Hz. This characteristic is a signature of the suspension dynamics [32].

Figure 7 shows the frequency response of the unladen truck compared with that of the loaded truck. Both the trucks performed the sinusoidal manoeuvres at 11.2 m/s (25 mph). From Figure 7, one can observe that the gain from steering input to y_{ZMP} exhibits a 10-dB increase for the laden vehicle versus the unladen vehicle; thus, the truck with the extra weight has higher y_{ZMP} magnitudes and thus a higher wheel-lift propensity than the unladen truck. Furthermore, the peak in the y_{ZMP} plot corresponding to the vehicle's roll mode shifts to lower frequencies as the vehicle is more heavily loaded. From the phase plot, it can be seen that the phase of the loaded vehicle lags behind that of the unladen truck for the whole frequency range. These results are in agreement with intuition: the loaded truck has much more inertia, thus making it slower to respond to the high-frequency inputs when compared with a lighter vehicle.

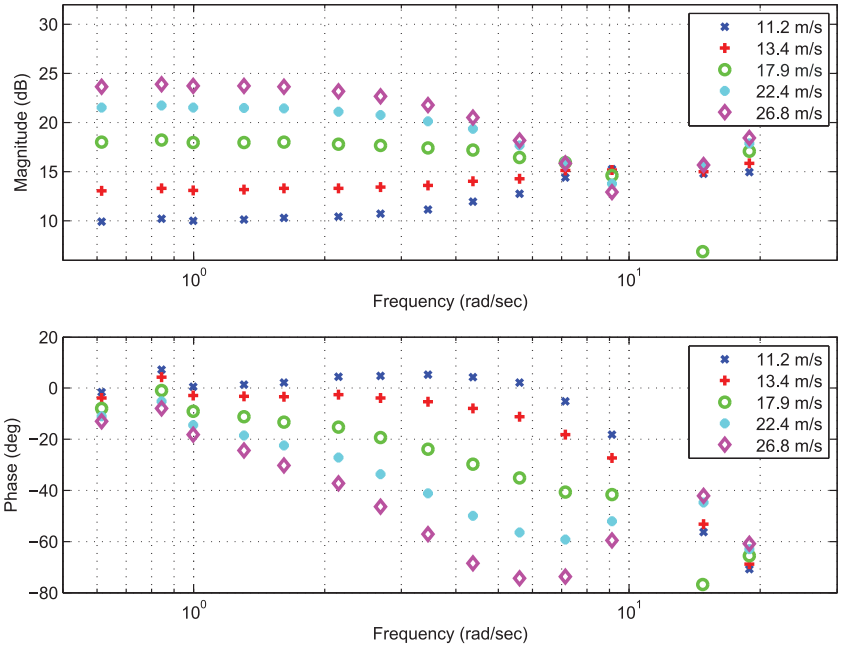

Figure 6. Frequency responses from road-wheel steering angle to y_{ZMP} of the unladen truck, flat road, with changing velocities.

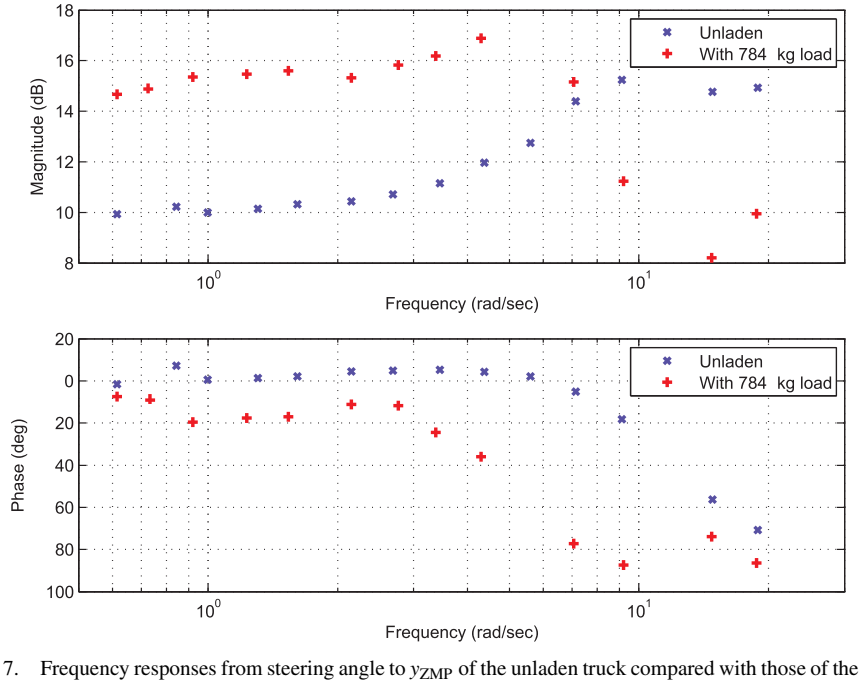

Figure 7. Frequency responses from steering angle to y_{ZMP} of the unladen truck compared with those of the loaded truck.

Next, the effect of road bank angle on the vehicle's rollover propensity was determined. For this analysis, the frequency responses of the unladen truck performing sinusoidal steering manoeuvres on a flat road and banked surface of 7° were taken into account. Both were simulated using CarSim at a velocity of 11.2 m/s. The results are shown in Figure 8.

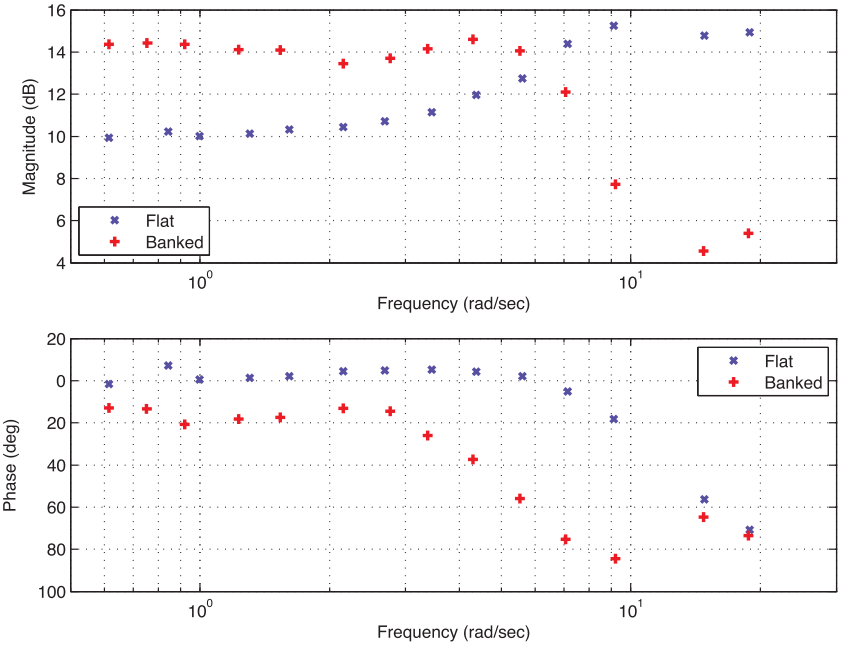

Figure 8. Frequency responses from steering angle to y_{ZMP} of the unladen truck on a flat road and a banked surface at the longitudinal velocity of 11.2 m/s.

As expected, the truck on the banked surface is more likely to roll over, especially for low frequencies. The frequency response on a banked surface will include both on-camber and off-camber tyre responses, and generally the on-camber response would be expected to reduce the gain. The net increase in the y_{ZMP} gain observed in the banked road plot thus stems from the half of the sinusoidal response in which the vehicle is turning up the road (similar to an off-camber turn). Interestingly, the y_{ZMP} responses of the unladen truck on the banked surface were very similar to those of the laden truck on a flat surface. This similarity may be a coincidence; however, if it is not, then one might be able to use the evaluation of the rollover propensity of top-loaded vehicles as a surrogate for testing normal vehicles' manoeuvring on banked roads. Further study of this similarity is certainly warranted given the large number of rollover accidents that occur on banked shoulder and median surfaces.

Although the proposed ZMP approach cannot analytically determine whether the vehicle will roll over or not, it gives an engineer a metric for evaluating a vehicle's rollover margin to determine whether a design is improved or worsened from a rollover perspective compared with a baseline design. This approach also highlights the rollover mode of the vehicle which allows the engineer to understand what the particular frequency that dominates the rollover mode of the vehicle is, so he or she can modify the configuration and/or properties of the vehicle suspension accordingly to reduce the likelihood of vehicle rollover. While this is important information, it is also important to consider the case where skidding occurs before wheel lift and precludes the possibility of vehicle rollover.

6. Using skid criteria for the calculation of worst-case wheel-lift steering inputs

To extend the use of the ZMP for design even further, we now review the method presented in [8] to determine the skid-before-roll condition. This is modified from the original study to

include the y_{ZMP} calculation of the vehicle. After using the method presented in Section 5 to determine the effects of a design or environmental change, an engineer can use the following procedure to examine worst-case steering manoeuvres for one particular scenario.

(1) Using a vehicle dynamic model or experimental measurements from a vehicle, find the frequency-domain relationship between steering angle and tyre slip, $\alpha(\omega)/\delta(\omega)$.
(2) Using results from (1) and a linear approximation to a nonlinear tyre model, estimate a representative tyre slip angle at which skidding occurs ($\alpha_{max,skid}$).
(3) Using the results of (1) and (2) at various steering frequencies (w), calculate the maximum steering possible that leads to tyre skidding, $|\delta|_{max,skid}$, as a function of w.
(4) Again, using a vehicle dynamic model, find the frequency-domain relationship between steering input and y_{ZMP}, $y_{ZMP}(\omega)/\delta(\omega)$. Using the ZMP threshold for wheel lift, calculate the maximum steering input that does not lead to wheel lift, $|\delta|_{max,roll}$, as a function of frequency.
(5) Plot the two different steering thresholds from (3) and (4) versus frequency, w. Wheel lift is predicted to occur at any location on the plot where the ZMP threshold is lower than the skidding threshold.

By looking at the resulting skid-before-roll plot, one can readily determine the frequencies at which the vehicle will be in a skid-before-roll condition. This analysis is discussed in the following sections using a simple roll model to facilitate the frequency-domain calculations.

7. A low-order vehicle roll model

The previous y_{ZMP} calculations depend on measures of the vehicle state during a manoeuvre and thus can be calculated either from experimental measurements or from models. Previous analyses used experimental measurements or CarSim simulations, both of which are quite difficult to obtain relative to simulation of linear models. To illustrate that the ZMP calculations from simple models are also quite valuable, a low-order linear model is introduced. The linear model used in this analysis assumes that all parts of the vehicle are rigid bodies, the vehicle is front wheel steered, the input to the system is the front wheel angle as measured at the road (as opposed to the handwheel angle), there is no pitch motion, tyre forces are proportional to the slip angle, the vehicle is moving at a constant velocity, the vehicle's sprung and unsprung mass centres both lie at a distance a from the front axle, the roll centre is fixed with respect to the vehicle's body, and the unsprung mass rotates only in the yaw direction. The coordinate system used in this model is shown in Figure 9. The model developed is mathematically consistent with the one developed in [33], except for the location of the vehicle coordinate system.

The angular velocity of the vehicle sprung mass can be expressed by the following vector quantity, in accordance with the aforementioned assumptions:

$$\vec{\omega}_s = r\hat{k} + \dot{\phi}\hat{\imath}, \tag{4}$$

while the vehicle's unsprung mass has an angular velocity of

$$\vec{\omega}_u = r\hat{k}. \tag{5}$$

If the velocity of the unsprung mass is defined as

$$\vec{v}_u = U\hat{\imath} + V\hat{\jmath}. \tag{6}$$

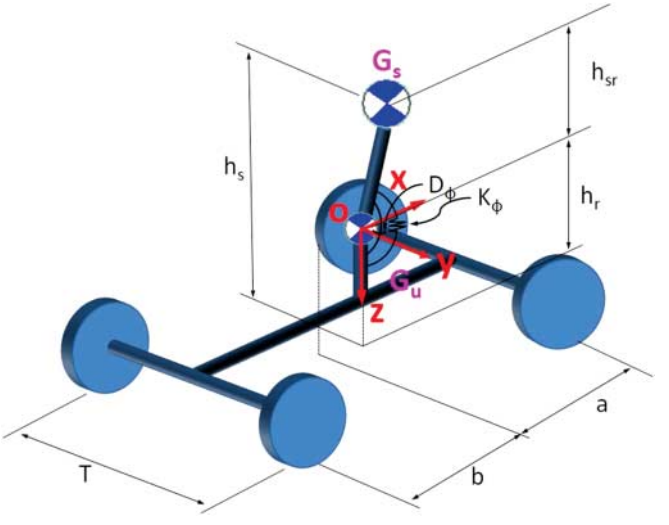

Figure 9. Standard SAE vehicle coordinate system.

Assuming small roll angles ϕ, the velocity of the sprung mass can be written using the familiar relative velocity equations:

$$\vec{v}_{\mathrm{s}} = U\hat{\imath} + (V + h_{\mathrm{sr}}\dot{\phi})\hat{\jmath}, \tag{7}$$

assuming that h_{sr} is defined as a positive quantity and the vehicle's roll centre is coincident with the unsprung mass CG. Differentiating each of these velocities and recalling that for any rotating basis vector $\hat{e}_i$, $\dot{\hat{e}}_i = \vec{\omega} \times \hat{e}_i$, one obtains the following expressions for the Newtonian accelerations of the sprung and unsprung masses of the vehicle:

$$\vec{a}_{\mathrm{s}} = -(V + h_{\mathrm{sr}}\dot{\phi})r\hat{\imath} + (\dot{V} + Ur + h_{\mathrm{sr}}\ddot{\phi})\hat{\jmath}, \tag{8}$$

$$\vec{a}_{\mathrm{u}} = -Vr\hat{\imath} + (\dot{V} + Ur)\hat{\jmath}. \tag{9}$$

Summing up of the external forces on the kinematic chain yields the following equation of motion in the y-direction:

$$m(\dot{V} + Ur) + m_{\mathrm{s}}h_{\mathrm{sr}}\ddot{\phi} = F_{\mathrm{f}} + F_{\mathrm{r}}. \tag{10}$$

Summing up of the moments about the vehicle's roll centre in the $\hat{\imath}$ direction and assuming that the vehicle's roll centre is close to the ground, the second equation of motion becomes

$$\sum M_{x,\mathrm{RC}} = I_{xx}\ddot{\phi} - I_{xz}\dot{r} + m_{\mathrm{s}}((-h_{\mathrm{sr}}\hat{k}) \times (\vec{a}_{\mathrm{s}})) \cdot \hat{\imath}, \tag{11}$$

$$-D_{\phi}\dot{\phi} + (m_s g h_{sr} - K_{\phi})\phi = I_{xx}\ddot{\phi} - I_{xz}\dot{r} + m_s h_{sr}(\dot{V} + Ur + h_{sr}\ddot{\phi}). \tag{12}$$

For the last equation, a moment balance in the yaw direction is taken about the sprung mass CG:

$$\sum M_{z,s} = I_{zz}\dot{r} - I_{xz}\ddot{\phi} + m_{\mathrm{s}}((-h_{\mathrm{sr}}\hat{k}) \times (\vec{a}_{\mathrm{s}})) \cdot \hat{k}, \tag{13}$$

$$aF_{\mathrm{f}} - bF_{\mathrm{r}} = I_{zz}\dot{r} - I_{xz}\ddot{\phi}. \tag{14}$$

This dynamic roll model is easily represented in a compact symbolic notation of the form

$$M \cdot \ddot{q} + D \cdot \dot{q} + K \cdot q = F \cdot u_f, \tag{15}$$

where

$$q = \{y\ \psi\ \phi\}^{\mathrm{T}} \tag{16}$$

denotes the states in the MDK representation, which are the lateral position, yaw angle, and roll angle, respectively. With

$$M = \begin{bmatrix} m & 0 & m_{\mathrm{s}} \cdot h_{\mathrm{sr}} \\ 0 & I_{zz} & -I_{xz} \\ m_{\mathrm{s}} \cdot h_{\mathrm{sr}} & -I_{xz} & I_{xx} + m_{\mathrm{s}} \cdot h_{\mathrm{sr}}^2 \end{bmatrix}, \tag{17}$$

$$D = \begin{bmatrix} 0 & m \cdot U & 0 \\ 0 & 0 & 0 \\ 0 & m_{\mathrm{s}} \cdot U \cdot h_{\mathrm{sr}} & D_{\phi} \end{bmatrix}, \tag{18}$$

$$K = \begin{bmatrix} 0 & 0 & 0 \\ 0 & 0 & 0 \\ 0 & 0 & K_{\phi} - m_{\mathrm{s}} \cdot g \cdot h_{\mathrm{sr}} \end{bmatrix}. \tag{19}$$

The input to the model

$$u = \{F_{\mathrm{f}}\ F_{\mathrm{r}}\}^{\mathrm{T}} \tag{20}$$

denotes the front and rear lateral tyre forces, respectively, so that

$$F = \begin{bmatrix} 1 & 1 \\ a & -b \\ 0 & 0 \end{bmatrix}. \tag{21}$$

This MDK form described by Equation (15) can be readily transformed to the general state-space form of

$$\frac{\mathrm{d}x}{\mathrm{d}t} = A \cdot x + B \cdot u \tag{22}$$

with the state vector

$$x = [V \quad r \quad \dot{\phi} \quad \phi]^T \tag{23}$$

representing the lateral velocity, yaw rate, roll rate, and roll angle, respectively. The transformation from the MDK form is straightforward by defining intermediate matrices:

$$M_{\mathrm{int}} = \begin{bmatrix} M & 0_{3x1} \\ 0_{1x3} & 1 \end{bmatrix}, \tag{24}$$

$$A_{\mathrm{int}} = \begin{bmatrix} -B & 0_{3x1} \\ 0_{1x3} & 1 \end{bmatrix} + \begin{bmatrix} 0_{3x3} & -K_{1-3,3} \\ 0\ 0\ 1 & 0 \end{bmatrix} + \begin{bmatrix} F \\ 0_{1x2} \end{bmatrix} \cdot \begin{bmatrix} C_{\alpha \mathrm{f}} & 0 \\ 0 & C_{\alpha \mathrm{r}} \end{bmatrix} \cdot \begin{bmatrix} \frac{1}{U} & \frac{a}{U} & 0 & 0 \\ \frac{1}{U} & -\frac{b}{U} & 0 & 0 \end{bmatrix}, \tag{25}$$

$$B_{\mathrm{int}} = \begin{bmatrix} F \\ 0_{1x2} \end{bmatrix} \cdot \begin{bmatrix} C_{\alpha \mathrm{f}} & 0 \\ 0 & C_{\alpha \mathrm{r}} \end{bmatrix} \cdot \begin{bmatrix} -1 \\ 0 \end{bmatrix}. \tag{26}$$

Then, the state-space matrices A and B are obtained from

$$\begin{aligned} A &= M_{\mathrm{int}}^{-1} \cdot A_{\mathrm{int}}, \\ B &= M_{\mathrm{int}}^{-1} \cdot B_{\mathrm{int}}. \end{aligned} \tag{27}$$

The state-space form more conveniently allows numerical simulation and frequency response calculations that are used in the following sections. One particular output of interest is the

dynamic relationship between steering angle and tyre slip, given for this vehicle model by

$$\alpha_{\mathrm{f}} = \frac{V + a \cdot r}{U} - \delta_{\mathrm{f}}, \tag{28}$$

$$\alpha_{\mathrm{r}} = \frac{V - b \cdot r}{U}. \tag{29}$$

In the state-space form, these slip angles are obtained as the measured output by selecting the C and D matrices as

$$C_{\mathrm{front}} = \begin{bmatrix} \frac{1}{U} & \frac{a}{U} & 0 & 0 \end{bmatrix}, \tag{30}$$

$$C_{\mathrm{rear}} = \begin{bmatrix} \frac{1}{U} & \frac{-b}{U} & 0 & 0 \end{bmatrix}, \tag{31}$$

$$D_{\mathrm{front}} = [-1], \tag{32}$$

$$D_{\mathrm{rear}} = [0]. \tag{33}$$

Also, the equations for y_{ZMP} presented in Section 4 linearise and simplify to the following:

$$y_{\mathrm{ZMP,lin}} = -\frac{I_{xx}}{mg}\ddot{\phi} + h_{\mathrm{sr}}\phi - \frac{h_{\mathrm{sr}}}{g}a_{y,\mathrm{CG}}. \tag{34}$$

This can be written as a state-space output matrix for the state-space model given in Equation (22) if the unsprung mass is considered to be sufficiently small and the equation for a_y given in Equation (9) is employed.

8. Fidelity of the low-order model

The low-order model's state predictions for a 50 km/h double-lane change manoeuvre are compared with a commercial vehicle simulation software (CarSim) and the Mammar third-order roll model in Figure 10. Though one particular model is shown, any model could be used as long as the equation used for y_{ZMP} makes use of the correct, Newtonian acceleration of the vehicle's centre of gravity. The comparison of the low-order model and CarSim, using the same vehicle parameters for both, showed a good agreement, particularly for the yaw rate, roll rate, and roll angle. The lateral velocity agreement was not as good as the above-mentioned one; however, the magnitudes of the responses were similar. The agreement in magnitudes is particularly important because the y_{ZMP} calculation depends especially on the magnitudes of the state vectors.

9. Skid-before-roll calculation

In this section, the procedures outlined in Section 6 are used to calculate the worst-case steering inputs for several vehicle situations. To begin, the transfer function of steering angle to slip angle in the frequency domain must be determined, and the easiest method is to obtain this from the state-space equations of the low-order vehicle model. Given a definition of the maximum allowable slip angle of each tyre that will lead to skidding of the tyre, $\alpha_{\max}$, the

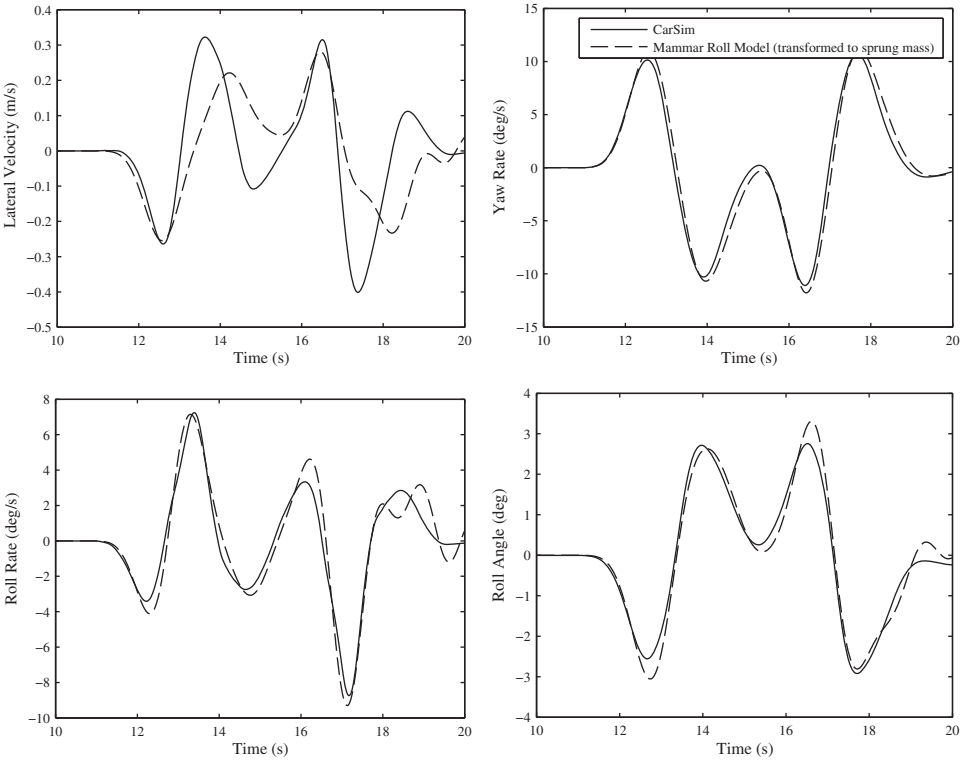

Figure 10. CarSim versus Mammar roll model.

maximum steering angle that can be generated in the model prior to causing a tyre to skid, $|\delta|_{\max,\text{skid}}(\omega)$, is given by

$$|\delta|_{\max,\text{skid}}(\omega) = |\alpha|_{\max} \cdot \left(\left| \frac{\alpha(\omega)}{\delta(\omega)} \right| \right)^{-1}, \tag{35}$$

where $\alpha(\omega)/\delta(\omega)$ is the complex frequency response of the system model from steering input to slip angle of the front or the rear tyre.

This approach is based on several assumptions, namely that the system response is sufficiently linear to allow frequency-by-frequency inversion of the model response and that the definition of skidding can be established by a numerical bound on tyre slip alone. Both assumptions are highly questionable given the vehicle state at the time of wheel lift. For example, as shown in Figure 11, the typical slip curve of an sport utility vehicle (SUV) tyre in CarSim does not have a clear location where one can definitely say that a tyre has 'started' to skid. However, using a saturated linear tyre model fit that captures the cornering stiffness and peak tyre force from a more complex model or actual tyre data, the maximum slip angle before skidding occurs can be approximated to a reasonable degree. From the simulated tyre curve for the tyres used on the GMC test truck, we hereafter approximate the maximum slip angle prior to skidding, $\alpha_{\max,\text{skid}}$, to be 10° for the particular tyres (front and rear) used for the test vehicle in question and for the *average normal load* that each carries. From this maximum slip angle, one can calculate the maximum steering angle before slipping for various frequencies, limited by either the front or the rear tyre slip, using Equation (35). Using parameters of the laden test truck, a representative plot is shown in Figure 12 of the maximum road-wheel steering

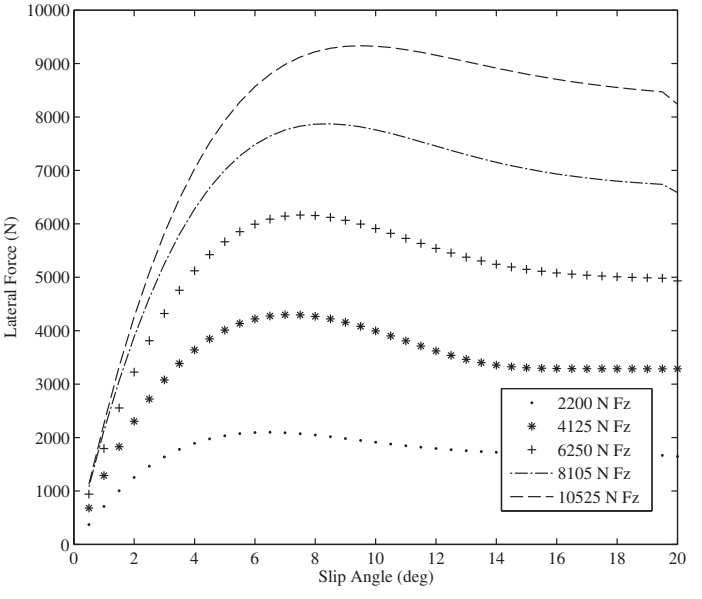

Figure 11. The definition of skidding from a tyre's force–slip curve.

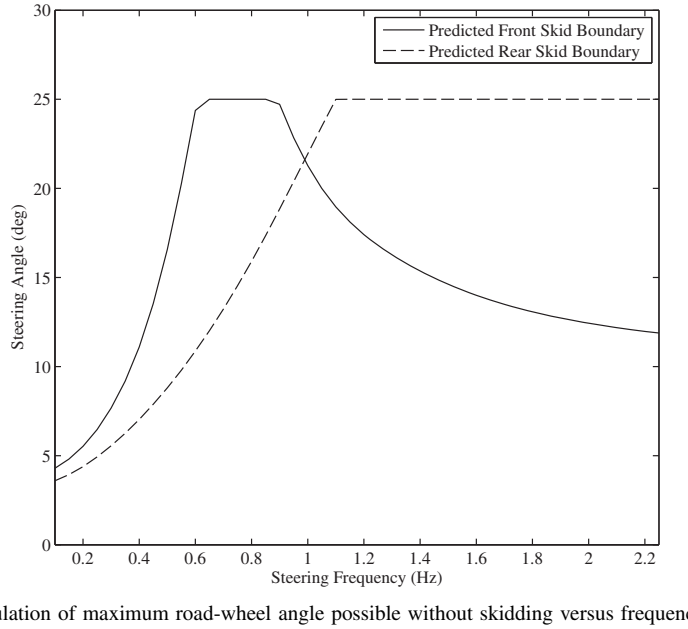

Figure 12. Simulation of maximum road-wheel angle possible without skidding versus frequency for laden test truck at 20 m/s.

angle available without causing tyre skidding for the laden GMC test vehicle at 20 m/s. At any given frequency, the actual maximum steering amplitude before skidding is determined by the minimum of the two curves. The front steering angle saturates at 25° due to the limits imposed by the steering rack.

Once the frequency-dependent maximum steering amplitude is known, the relationship between the maximum value of y_{ZMP} and steering angle can be found. Similar to the

maximum skid angle, one can find the frequency response between steering input and y_{ZMP}, $y_{ZMP}(\omega)/\delta(\omega)$. Assuming that the support polygon of the typical vehicle is a rectangle that has a width equal to the track width of the vehicle, the maximum y_{ZMP} value allowable prior to wheel lift is simply one half of the vehicle track width. The maximum steering angle before entering the roll condition is found by dividing the maximum y_{ZMP} by the transfer function of the steering angle to y_{ZMP}. It is important to note that the current state of the ZMP method used for predicting wheel lift cannot determine precisely which wheel will lift. Inclusion of an x_{ZMP} calculation might be able to provide this, but the authors feel that for conservative vehicle design, knowledge that any wheel lift is imminent is sufficient:

$$|\delta|_{\max,\text{roll}}(\omega) = |y_{ZMP}|_{\max} \cdot \left(\left| \frac{y_{ZMP}(\omega)}{\delta(\omega)} \right| \right)^{-1}, \tag{36}$$

where $y_{ZMP}(\omega)/\delta(\omega)$ is the complex frequency response of the system model from steering input to y_{ZMP} of the vehicle, calculated from the vehicle model and Equation (3). Because the vehicle is not dynamically stable when the y_{ZMP} is outside the track width of the vehicle, the vehicle will begin to enter either a front wheel-lift or a rear wheel-lift condition.

Figure 13 shows the maximum steering angle possible before the y_{ZMP} predicts wheel lift, and the steering angle leading to skidding, again for the case of the laden vehicle at 20 m/s. In this simulation, one can see that the wheel-lift threshold is lower than the skidding threshold at a range of frequencies and, thus, wheel lift is predicted to occur for sinusoidal inputs at these frequencies.

The previous results show the slide before roll condition at one speed. Because of the ease in using this analysis, the ZMP and skidding results can be calculated and compared for speeds from 10 to 40 m/s, speeds in the common operating range for a passenger vehicle. Since we are most interested in the skid condition relative to the wheel-lift condition, Figure 14 only shows the minimum of both the front skid and the rear skid surfaces for comparison with the wheel-lift surface predicted by the ZMP method. From the contour plot shown in Figure 14,

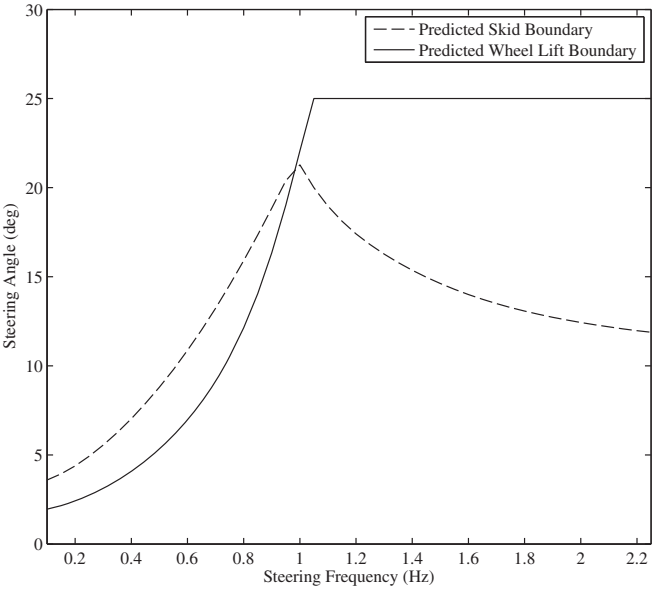

Figure 13. Maximum steering angle possible without wheel lift or skidding versus frequency for laden test truck at 20 m/s.

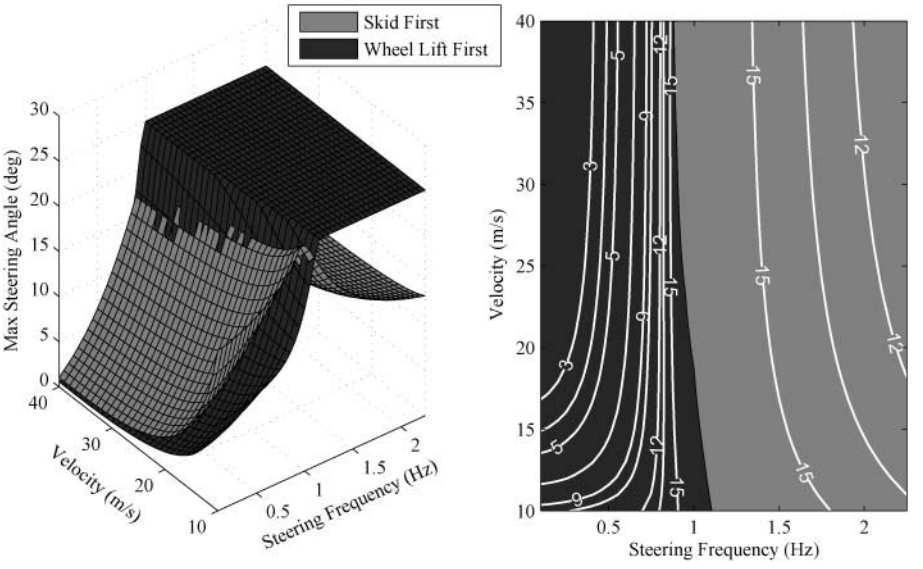

Figure 14. Maximum steering angle possible without wheel lift or skidding versus frequency and vehicle speed.

it is easy to see that the smallest amplitude wheel-lift condition will occur at low frequencies, and the smallest steering amplitude causing wheel lift occurs along the 3° road-wheel angle isoline, which spans 10–40 m/s and 0–0.5 Hz. One can also observe that as the speed increases, a lower steering angle is required to induce wheel lift in the vehicle.

The previous analysis considered the smallest steering amplitude leading to wheel lift. Another definition of a worst-case steering manoeuvre would be the one that has the largest margin between wheel lift and skidding. This margin can be readily obtained by subtracting the minimum skid condition from the wheel-lift condition to obtain a surface of the margin of safety between the two conditions. Here, a negative value indicates a wheel-lift condition and a positive value indicates a skid condition. The results are shown in Figure 15. One can observe that wheel lift will occur at lower frequencies (below 1 Hz). From the contour plot, the conditions giving the most negative margin of steering amplitude between rollover and skidding occur at 10 m/s and 0–0.9 Hz. The occurrence of wheel lift prior to wheel slip at low frequencies is governed by the difference between the roll amplitude and the amount of tyre slip, as shown in Figure 13. The roll dynamics are greatly influenced by the expected parameters: CG height, wheelbase, track width, and mass, but also I_{xx} to some degree. The tyre slip is governed especially by the bicycle model dynamics of the vehicle. The ZMP results highlight the interplay between these two responses and why simple analytical rules for predicting wheel lift are so hard to generalise across all vehicles and driving situations.

These analyses have highlighted particular frequencies of concern for rollover for a given speed and a given vehicle, but these predictions are formed from a linear model and very simplistic definition of skidding. It is important to mention the inherent limitations of this method. The assumption that the tyres are represented well by a saturated linear model is questionable at the conditions of impending skid. Additionally, the roll model for the vehicle is relatively simplistic, and the assumption of linearity for determining skid-before-roll behaviour is based on a steady-state, linear response to a sinusoidal steering input. For high frequencies especially, it may be extremely difficult to bring about wheel lift without rather violent steering motions, and the nonlinearities in the model will be pronounced. All these assumptions may negate any value of a linear analysis or they may collectively cancel to produce net minor

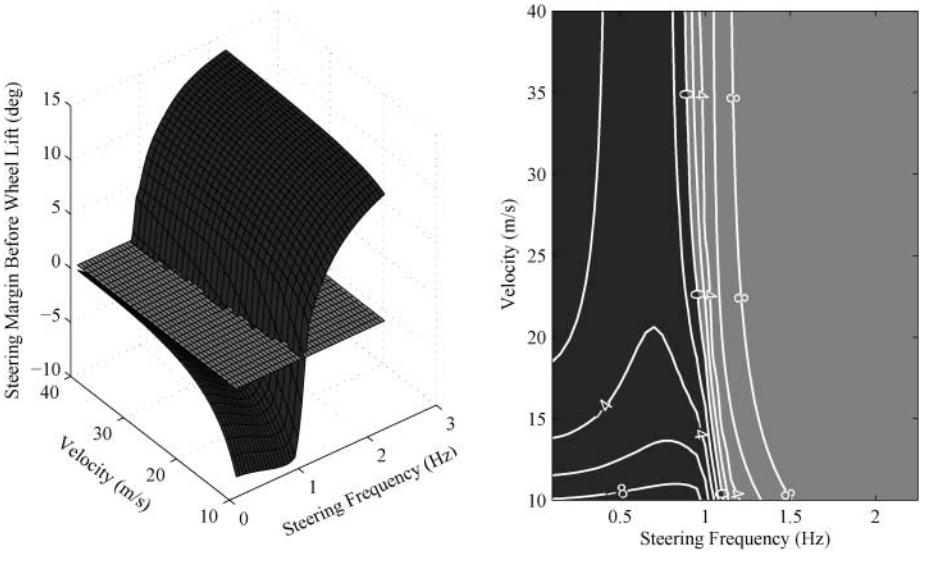

Figure 15. Margin of steering angle between wheel lift and skidding versus frequency and vehicle speed.

deviations that only have a small effect on the overall validity of the method. To determine which case is more descriptive, the linear model predictions can be compared with a more fully representative, but repeatable, data source.

To test the predictions given in the previous section, data that include the kinematic and tyre nonlinearities typically present in a vehicle for situations predicted to cause both skidding and wheel lift are needed. Again, CarSim was used to simulate the real vehicle and to test the fidelity of the proposed linear approach. Several test manoeuvres were simulated in CarSim using sinusoidal steering inputs at various amplitudes and frequencies at 20 m/s around the 'safety boundary' predicted in Figure 16. For each test case, the steady-state behaviour of the vehicle was analysed to look for both wheel-lift and tyre lateral force saturations. For example, for 20 m/s forward speed and a 0.9 Hz steering input at 15° of road-wheel angle, CarSim predicts wheel lift. F_z for the front and rear tyres are shown in Figure 17.

As expected, during CarSim tests characterised by excessive wheel lift, the 'roll-*before*-skid' calculation is not exact. Wheel lift and skidding occur together as a consequence of the

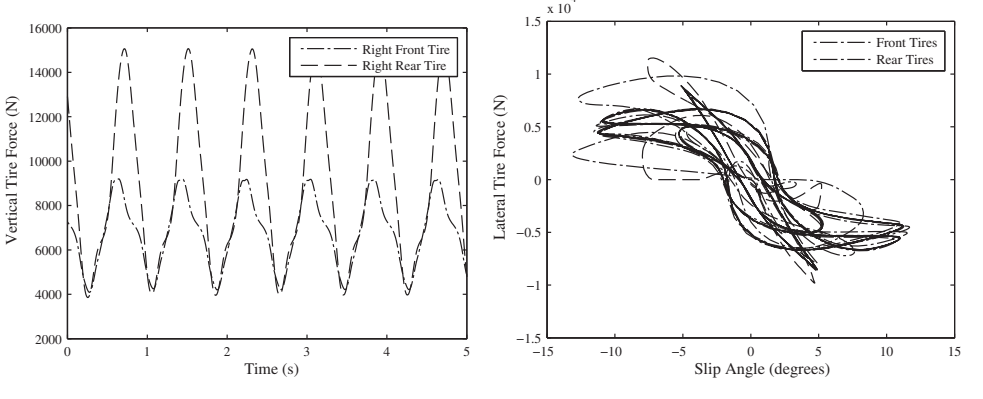

Figure 16. CarSim-predicted tyre forces: 20 m/s, 15° of steer at 1.25 Hz.

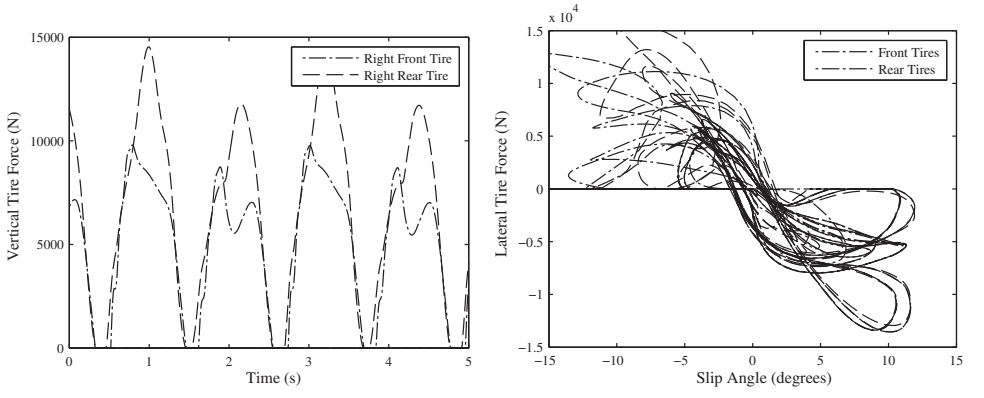

Figure 17. CarSim-predicted tyre forces: 20 m/s, 15° of steer amplitude sinewave at 0.9 Hz.

wheel-lift events. In cases where no wheel lift is observed, however, the presence of skidding behaviour is illustrated by plotting the lateral tyre force versus the slip angle for the tyres. Skidding behaviour is characterised by large departures from tyre force linearity. Also, since our definition of skidding in the calculation of the y_{ZMP} assumes that skidding occurs above 10°, any CarSim test in which slip angles of 10° or greater are observed is considered a skid case.

In this way, a suite of tests with CarSim helped illustrate the fidelity of the approach to determining worst-case steering manoeuvres outlined in Section 7. The agreement between CarSim and the skid-before-roll approach is shown in Figure 18. One can observe in Figure 18 that, especially at frequencies greater than 1 Hz, skidding occurs at amplitudes slightly less than those predicted, and this is possibly due to a poor definition of the skidding threshold. However, the trends and approximate numerical boundaries for both wheel-lift and skid events are captured by the linear ZMP analysis.

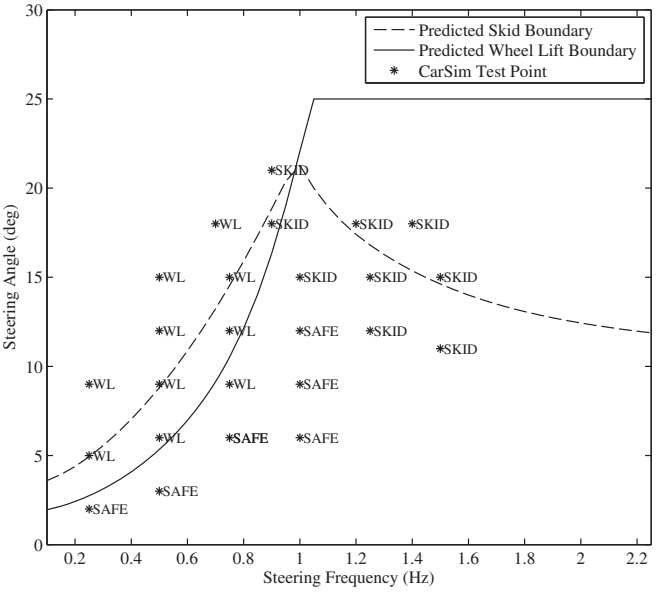

Figure 18. Skid-before-roll results for various steering inputs at 20 m/s for the laden GMC test truck.

Although the method works for one particular rollover-prone vehicle configuration, others should also be tested. CarSim's standard 'large SUV' vehicle was tested to show how well the skid-before-roll calculation performs for a stock production vehicle. The results of the skid-before-roll analysis for this vehicle are shown in Figures 19 and 20 .

While the skid-before-roll analysis does suggest that this vehicle will lift a wheel, CarSim simulations do not show wheel lift for any steering frequency or amplitude. This does not necessarily indicate that the ZMP is in error – the test cases illustrated in Figure 20 exhibited extremely low normal tyre loads, as little as 10 N in some cases. This indicates that while the vehicle does not technically lift a wheel, the configuration is dangerously close to wheel lift at certain steering frequencies. Again, the aim of the skid-before-roll method is to provide

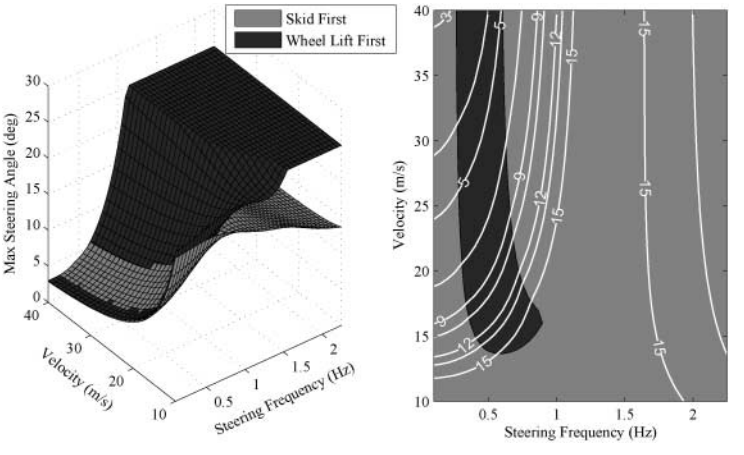

Figure 19. Skid-before-roll results for various steering inputs for the large SUV.

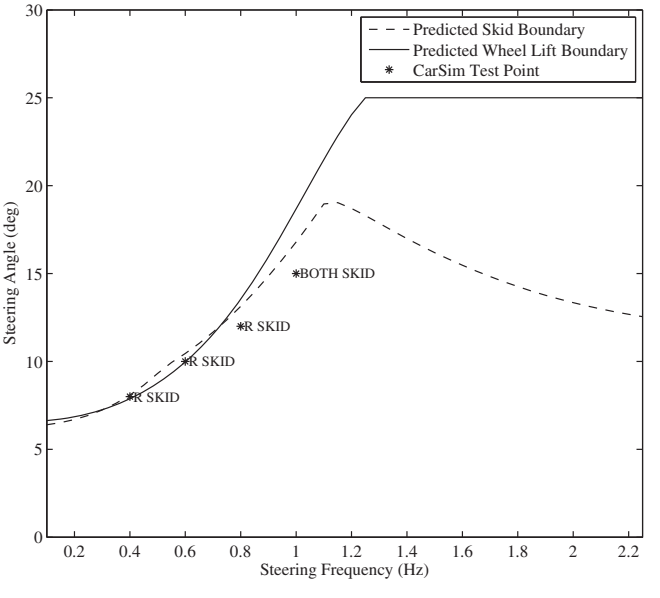

Figure 20. Skid-before-roll results for various steering inputs at 20 m/s for the large SUV.

quantitative insights into what manoeuvres offer the greatest safety risk for a particular vehicle design.

Despite the inherent assumptions of the model, the CarSim results show that the skid-before-roll calculation generally predicts both the trends and the steering magnitudes leading to wheel lift and skidding under various steering amplitudes, frequencies, and speeds. Additionally, it gives an indication of the worst-case steering situations.

These worst-case manoeuvres in the frequency domain can greatly inform the time-domain testing profiles. To better illustrate this point, consider the CarSim results from a standard NHTSA 'Toyota J' fishhook manoeuvre shown in Figure 21. When compared with the predicted tyre normal loads from the first moments of a 0.5 Hz 9° sinusoidal road-wheel input in Figure 21, it is clear that the Toyota J turn does *not* represent a 'worst-case' steering input for this particular vehicle. The skid-before-roll calculation predicts that the sinusoidal input shown in Figure 22 would be worse, and indeed a CarSim simulation of this manoeuvre provides

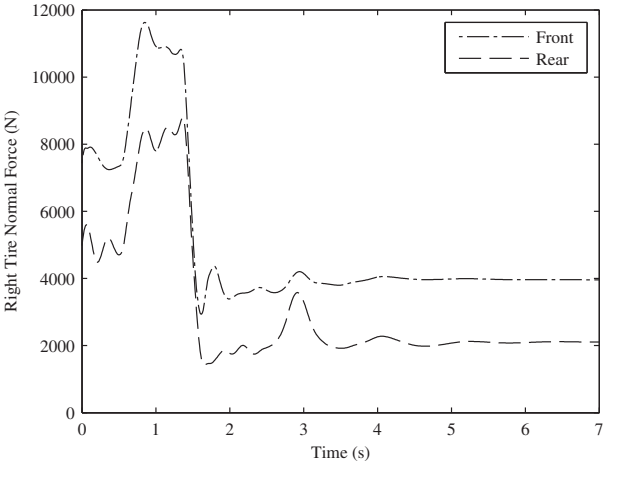

Figure 21. CarSim-predicted tyre normal loads for an 80 km/h 'Toyota J' turn.

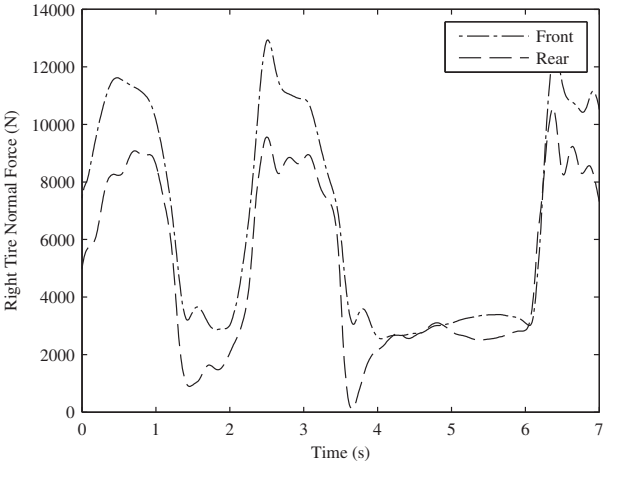

Figure 22. CarSim-predicted tyre normal loads for a 0.5 Hz 9° sinusoidal steering input at 20 m/s.

confirmation that not only is the manoeuvre much worse than a Toyota J turn, but also this particular vehicle is alarmingly close to exhibiting wheel lift.

It is also worth mentioning that for the CarSim 'standard large SUV', the skid curve that follows the wheel-lift curve in Figure 20 is for the *rear* tyres at low frequencies. Trading rear-tyre skid for potential wheel lift might not be an acceptable design trade-off. While the CarSim results suggest that the 'standard large SUV' remains stable even in the face of these short-duration rear-tyre skids, a split-μ scenario or small perturbations in vehicle inputs or environmental conditions could have disastrous results.

10. Conclusions

In this paper, an approach to evaluate vehicle rollover propensity has been proposed using the ZMP methodology. This methodology utilises the ZMP and frequency responses as tools to determine the rollover margin of a vehicle. Using a simulated vehicle model, the effectiveness of the approach was examined across different scenarios. From the results, it is evident that a vehicle has a higher likelihood of rollover once it travels at higher speeds. Moreover, at lower speeds, the excitation frequency slightly has an effect on the rollover margin. For the case of the loaded truck, the results show that the gain between steering input and stability margin changes as expected. Furthermore, the vehicle driven on a banked surface has more risk of rollover than that driven on a flat road. Even though some of the results seem to be somewhat obvious and follow intuition, this approach gives a qualitative tool to judge the risk of rollover among vehicles.

The qualitative results of the ZMP calculation in the frequency domain were then extended using the ZMP to calculate a skid-before-roll condition. This model-based analysis was used to predict worst-case steering situations for several different vehicle configurations. Comparisons between this approach and a high-fidelity simulation software package showed a very good agreement, even when skidding and wheel lift occurred simultaneously. Finally, the skid-before-roll approach was able to identify manoeuvres that resulted in reduced rollover margins when compared with the standard 'Toyota J' manoeuvre currently used to evaluate a vehicle's rollover propensity.

Acknowledgements

The authors thank the Thomas D. Larson Pennsylvania Transportation Institute for the financial support. Sittikorn Lapapong cordially thanks the Ministry of Science and Technology, the Royal Thai Government, for the financial support.

References

[1] National Highway Traffic Safety Administration, *Traffic safety facts 2008 – a compilation of motor vehicle crash data from the fatality analysis reporting system and the general estimates system*, U.S. Department of Transportation, Washington, DC, 2009.

[2] S. Lapapong and S. Brennan, *Terrain-aware rollover prediction for ground vehicles using the zero-moment point method*, Proceedings of the American Control Conference, Baltimore, MD, June 2010, pp. 1501–1507.

[3] S. Lapapong, A.A. Brown, and S.N. Brennan, *Experimental validation of terrain-aware rollover prediction for ground vehicles using the zero-moment point method*, Proceedings of the 10th International Symposium on Advanced Vehicle Control (AVEC2010), Vol. 2, Longsborough, UK, August 2010, pp. 1233–1237.

[4] S. Lapapong, *Vehicle rollover prediction for banked surfaces*, Ph.D. diss., The Pennsylvania State University, 2010.

[5] S. Lapapong and S.N. Brennan, *A novel comparative approach to evaluate vehicle rollover propensity*, Proceedings of 2011 IAVSD, Manchester, England, August 2011.

[6] M. Vukobratović and D. Juričić, *Contribution to the synthesis of biped gait*, Proceedings of IFAC Symposium, Technical and Biological Problem on Control, Erevan, USSR, 1968.
[7] R.D. Ervin and Y. Guy, *The influence of weights and dimensions on the stability and control of heavy-duty trucks in Canada* Vol. I, Tech. Rep. UMTRI-86-35/I, The University of Michigan Transportation Research Institute, Ann Arbor, MI, July 1986.
[8] J.T. Cameron, *Vehicle dynamic modeling for the prediction and prevention of vehicle rollover*, Master's thesis, The Pennsylvania State University, 2005.
[9] G.J. Forkenbrock, B.C. O'Harra, and D. Elsasser, *A demonstration of the dynamic tests developed for nhtsas ncap rollover rating system – Phase viii of nhtsas light vehicle rollover research program*, Tech. Rep. DOT HS 809 705, NHTSA/NVS-312, Washington, DC, 2004.
[10] Transportation Research Board, *The National Highway Traffic and Safety Administration's Rating System for Rollover Resistance*, National Academy Press, Washington, DC, 2002.
[11] T.J. Wielenga and M.A. Chace, *A study in rollover prevention using anti-rollover braking*, SAE Tech. Paper Series, no. 2000-01-1642, Society of Automotive Engineers, Inc., Warrendale, PA, 2000.
[12] B.-C. Chen and H. Peng, *Differential-braking-based rollover prevention for sport utility vehicle with human-in-the-loop*, Veh. Syst. Dyn. 36(4–5) (2001), pp. 359–389.
[13] C.R. Carlson and J.C. Gerdes, *Optimal rollover prevention with steer by wire and differential braking*, Proceedings of the 2003 ASME IMECE, Vol. 72 DSC, no. 1, Washington, DC, November 2003, pp. 345–354.
[14] J. Yoon, D. Kim, and K. Yi, *Design of a rollover index-based vehicle stability control scheme*, Veh. Syst. Dyn. 45(5) (2007), pp. 459–475.
[15] R.V. Dukkipati, J. Pang, M.S. Qatu, G. Sheng, and Z. Shuguang, *Road Vehicle Dynamics*, Society of Automotive Engineers, Inc., Warrendale, PA, 2008.
[16] S.C. Peters and K. Iagnemma, *Stability measurement of high-speed vehicles*, Veh. Syst. Dyn. 47(6) (2008), pp. 701–720.
[17] G.J. Heydinger, R.A. Bixel, W.R. Garrott, M. Pyne, J.G. Howe, and D.A. Guenther, *Measured vehicle inertial parameters-NHTSA's data through november 1998*, SAE Tech. Paper Series, no. 1999-01-1336, Society of Automotive Engineers, Inc., Warrendale, PA, 1999.
[18] P. Sardain and G. Bessonnet, *Forces acting on a biped robot. Center of pressure–zero moment point*, IEEE Trans. Syst. Man Cybern. A 34(5) (2004), pp. 630–637.
[19] M. Vukobratović and B. Borovic, *Zero-moment point – Thirty five years of its life*, Int. J. Humanoid Robot. 1(1) (2004), pp. 157–173.
[20] M. Vukobratović and B. Borovic, *Dynamic control of unstable locomotion robots*, Math. Biosci. 24 (1975), pp. 129–157.
[21] M. Vukobratović, B. Borovic, D. Surla, and D. Stolić, *Biped Locomotion: Dynamics, Stability, Control, and Application*, Spring, Berlin, Germany, 1990.
[22] K. Hirai, M. Hirose, Y. Haikawa, and T. Takenaka, *The development of Honda humanoid robot*, Proceedings of the IEEE International Conference on Robotics and Automation, Vol. 2, Leuven, Belgium, May 1998, pp. 1321–1326.
[23] S. Sugano, Q. Huang, and I. Kato, *Stability criteria in controlling mobile robotic systems*, Proceedings of the IEEE International Conference on Intelligent Robots and Systems, Tokyo, Japan, July 1993, pp. 832–838.
[24] Q. Huang and S. Sugano, *Manipulator motion planning for stabilizing a mobile-manipulator*, Proceedings of the IEEE International Conference on Intelligent Robots and Systems, Vol. 3, Pittsburgh, PA, August 1995, pp. 467–472.
[25] H. Baruh, *Analytical Dynamics*, McGraw-Hill Book Co., Singapore, 1999.
[26] A. Dasgupta and Y. Nakamura, *Making feasible walking motion of humanoid robots from human motion capture data*, Proceedings of the IEEE International Conference on Robotics and Automation, Vol. 2, Detroit, MI, May 1999, pp. 1044–1049.
[27] J. Kim and W.K. Chung, *Real-time zero moment point compensation method using null motion for mobile manipulators*, Adv. Robot. 20(5) (2006), pp. 581–593.
[28] J.L. Meriam and L.G. Kraige, *Engineering Mechanics: Dynamics*, 4th ed., Wiley, New York, 1997.
[29] P.E. Wellstead, *Frequency response analysis*, Tech. Rep. 10, Solartron Instruments, Hampshire, UK, 2003.
[30] E. Laubwald and M. Readman, *Frequency response analysis*, Cheshire, UK, Technical Report, available at http://www.control-systems-principles.co.uk/downloads.html.
[31] J.S. Stine, B.C. Hamblin, S.N. Brennan, and E.T. Donnell, *Analyzing the influence of median cross-section design on highway safety using vehicle dynamics simulations*, Accid. Anal. Prev. 42(6) (2010), pp. 1169–1777.
[32] S. Lapapong, A.A. Brown, and S.N. Brennan, *Frequency characteristics and explanation of notches seen in frequency responses of vehicles*, Proceedings of the TSME International Conference on Mechanical Engineering, Krabi, Thailand, October 2011.
[33] S. Mammar, V.B. Baghdassarian, and L. Nouveliere, *Speed scheduled lateral vehicle control*, Proceedings of the International Conference on Intelligent Transportation Systems, 1999, pp. 80–85.